# The wheat VIH2-3B, a functional PPIP5K controls the localization of fasciclin-like arabinogalactan protein

**Author names and affiliations:**

Anuj Shukla[1,2,3], Reshma Gopal[1,4], Riya Ghosh[5], Ankur Chaudhuri[5], Kanupriya Agrwal[1], Rahul Tanwar[1], Henning Jacob Jessen[2,3], Debabrata Laha[5] and Ajay K Pandey[1,*]

[1]National Agri-Food Biotechnology Institute (Department of Biotechnology), Sector 81, Knowledge City, S.A.S. Nagar, Punjab, India.

[2] Institute of Organic Chemistry, University of Freiburg, Albertstraße 21, 79104, Freiburg, Germany.

[3]Centre for Integrative Biological Signalling Studies, University of Freiburg, 79104 Freiburg, Germany.

[4]Regional Centre for Biotechnology, Faridabad - 121001 Haryana (NCR), Delhi, India

[5]Department of Biochemistry, Indian Institute of Science, Bengaluru-560012, Karnataka, India

*Corresponding author:

Dr. Ajay K Pandey, Scientist-F

**Email:** pandeyak@nabi.res.in; pandeyak1974@gmail.com

**ORCID iD:** https://orcid.org/0000-0003-1064-139X

**Abstract**

Inositol pyrophosphates (PP InsPs) are important signalling molecules that participate in multiple physiological processes across a wide range of eukaryotes. Metabolic pathway kinases (VIP1/VIHs) leading to the production of PP-InsPs are now well characterized in yeast and plants. Previously, the wheat (*Triticum aestivum* L.) inositol pyrophosphate kinase (TaVIH2) was shown to encode a catalytic active kinase domain. Heterologous expression of TaVIH2 in *Arabidopsis thaliana* was shown to enhance drought tolerance by modulating the cell composition. In this study, we attempted to identify the interacting protein targets of wheat VIH2-3B using a yeast two-hybrid (Y2H) cDNA library screen, which led to the identification of 52 putative interactors that are primarily involved in cell wall-related functions. Notably, fasciclin-like arabinogalactan protein (FLA7), a glycosylphosphatidyl inositol (GPI)-anchored protein, emerged as the most frequently interacting partner. Further analysis using pulldown assays validated the interaction between TaVIH2-3B and TaFLA7 in vivo. Using the reporter fusion studies, we observed the localization of TaFLA7 to be a plasma membrane and this localization of the TaFLA7 was perturbed in the yeast vip1Δ strain. The expression of TaVIH2-3B bearing PPIP5K enzymatic activity in yeast mutants rescued the level of $IP_8$ and restore the localisation of the TaFLA7 to the membrane. Expression analysis of TaFLA7 revealed a differential expression response to drought in wheat shoot tissues. TaFLA7 was also found to be highly expressed during grain development, particularly in the endosperm and seed coat during grain maturation. Taken together, these findings highlight the potential role of TaVIH2 in cell wall remodelling and stress response pathways, offering new insights into the functional roles of VIH proteins in plants.

**Key word:** Inositol pyrophosphates, kinases, cell wall maintenance.

## 1. Introduction

Inositol pyrophosphates (PP-InsPs) are high-energy molecules that are ubiquitous in various eukaryotic organisms and serve as critical cellular signaling entities (Szijgyarto et al. 2011). Over the last two decades, inositol pyrophosphate signalling has gained significant attention and has been proven to regulate different cellular functions such as regulating telomere length, DNA repair, phosphate homeostasis, vesicular trafficking and protein phosphorylation (Saiardi 2004; Fridy et al. 2007; Lee et al. 2007; Azevedo et al. 2009; Thota and Bhandari 2015; Shears 2015; Sanchez et al. 2019; Pipercevic et al. 2023; Chabert et al. 2023). Researchers have identified two distinct classes of inositol pyrophosphate synthases, inositol hexakisphosphate kinases (referred to as IP6Ks or Kcs1-like proteins) and diphosphoinositol pentakisphosphate kinases (known as PPIP5Ks or Vip proteins) (Choi et al., 2007). The latter kinases are primarily classified based on their catalytic specificity towards various positions on the inositol ring with a ATP-grasp domain at the C-terminal (Mulugu et al. 2007).

Genes encoding VIH-type PP-InsP synthase could be identified in green algae and embryophytes (Desai et al. 2014; Laha et al. 2015). *Arabidopsis* VIH proteins catalyze the synthesis of the inositol pyrophosphate, $InsP_8$ and VIH-derived $InsP_8$ has been linked with diverse physiological processes such as plant defence and phosphate homeostasis (Laha et al. 2016; Jung et al. 2018; Dong et al. 2019; Zhu et al. 2019; Ried et al. 2021; Riemer et al. 2021; Land et al. 2021) . It was further shown that $InsP_8$ binds to SPX1 protein and controls its interaction with the phosphate starvation response 1 (PHR1), a central regulator of phosphate starvation (Jung et al. 2018; Dong et al. 2019; Ried et al. 2021). Based on this evidence, one could speculate that PP-InsPs are associated with different physiological stress response signalling cascades.

Although the level of PP-InsPs seems to be important in asserting such function, it remains to be studied if the responsible kinases, especially plant VIH could interact physically with the components of the specific signalling system. One consequence could be local enrichment of PP-InsP species in the vicinity of their target proteins. There are multiple reports that suggests the employment of such gating of PP-InsP to its target proteins through physical interaction of the responsible PP-InsP synthase (Rao et al. 2014; Zhou et al. 2021; Laha et al. 2022; Bhandari et al. 2024). A comprehensive interaction study for the HIV protein is lacking in plants, which could provide new insights into how its signalling output is regulated. Multiple VIH proteins were identified in hexaploid wheat ((*Triticum aestivum* L.) with diphosphoinositol pentakisphosphate kinases (PPIP5K) like enzymatic activity

(Shukla et al. 2021). Notably, when wheat VIH homolog (TaVIH2-3B) was expressed heterologously in *Arabidopsis*, it conferred tolerance to drought conditions (Shukla et al. 2021). Further, it was shown that VIH2 overexpressed lines show reprogramming of genes involved in cell-wall-related metabolic pathways. At the metabolome level, these transgenic lines showed high accumulation of cell-wall cementing polysaccharides such as arabinoxylan and arabinogalactan (Shukla et al. 2021). Although the role of VIH was established in imparting drought tolerance in plants, it remains to be dissected if VIH could be involved at the protein level.

Using a yeast two-hybrid (Y2H) screening system, we identified multiple interactors of TaVIH2-3B. Further, a detailed characterisation was done for one of the interactors referred to as FLA7, which is involved in the cell wall maintenance process. Using biochemical experiments and a yeast genetic screen, we demonstrated that the presence of VIH-type PP-InsP synthase is required for FLA7 localisation. This study expands our knowledge of the functioning of the plant VIHs towards new roles, including cell wall homeostasis.

## 2. Materials and methods

### 2.1. Wheat cDNA library construction and yeast two-hybrid screening

Total RNA extracted from the wheat seedlings was used to purify mRNA. mRNA was isolated by a plant mRNA isolation kit (Sigma). The mRNA concentration and purity were checked by nanodrop and 0.8% (w/v) agarose gel, then visualized by ethidium bromide staining under UV transilluminator. Multiple batches of mRNA were pooled together to prepare the cDNA library, and single-strand cDNA was constructed as described in the materials and methods section. Next, the double-strand cDNA was prepared through long-distance PCR, and aliquots were analyzed on the 1.2% agarose ethidium bromide gel. Finally, the ds-cDNA was first purified using CHROMA SPIN+TE-400 columns. For yeast-two-hybrid experiments (Y2H), the wheat cDNA library was prepared by the co-transformation of the pGADT7-Rec vector (containing SV40 Nuclear Localization Sequence) provided in the kit (Matchmaker Gold Yeast Two-Hybrid System, Takara Bio, USA) and purified cDNA prepared in the Y187 yeast strain. The transformation mixture was diluted ($10^{-1}$ and $10^{-2}$), and 100 µl of each dilution was plated on the SD-L agar plates to select independent clones, indicating the readiness of our library's complexity. In total, approximately 1.2 million independent transformants were screened, corresponding to about 5× the estimated

complexity of the wheat cDNA library, ensuring a saturated screening for comprehensive identification of potential interacting partners. The full length TaVIH2 cDNA was cloned in the pGBKT7 vector using Sma1 and Not1 restriction sites.

**2.2. Quantitative real-time PCR**

To quantify the gene expression in roots, qRT-PCR was performed using the QuantiTect SYBR Green RT-PCR Kit (Qiagen, Germany). The gene-specific primers capable of amplifying the genes mentioned in TableS1 were carefully designed using Oligocalc software. The cDNA dilutions to be used were optimized by running a semi-quantitative PCR for 22-25 cycles using Thermo Scientific™ DreamTaq™ Green PCR Master Mix (2X). The qRT-PCR reaction was set up in a 96-well plate by mixing the reaction components including 1X QuantiTect SYBR Green RT-PCR Master Mix, appropriate cDNA dilution, 900nM of forward and reverse primers and MQ to final volume of 10µl in each well and the plate was run in 7500 Fast Real-Time PCR System. 4-5 technical replicates for each set of primers and a minimum of 2 biological replicates were used to validate the experiment. ADP-ribosylation factor gene (TaARF) was used as an internal control in all the expression studies (Meena et al. 2024). The Ct values obtained after the run were normalized against the internal control and relative expression was quantified using $2^{-\Delta\Delta CT}$ method (Livak and Schmittgen 2001).

**2.3.Bioinformatics and molecular docking analysis**

Intrinsic disorder region (IDR) percentage, length and position of human (*Homo sapiens*) and plant-encoded PPIP5K-like proteins were done using ESpritz (ver1.3) (Walsh et al. 2012). In silico protein-protein interaction was anlayzed using STRING analysis (Szklarczyk et al. 2023). For gene expression studies the expression browser from https://www.wheat-expression.com was used (Ramírez-González et al. 2018). Wheat eFP Browser (Triticum aestivum) cv. Azhurnaya developmental time course was used for the analysis of the gene expression at different Zadoks scale (Z) levels, which were summarised as TPM from the transcript to the gene level using tximport v1.2.0. Three biological replicates, consisting of five individual plants each. were sampled at the developmental times and tissues mentioned.

The complete protein sequences of FLA7 homoeologs FLA7-2A (TraesCS2A02G165600) and FLA7-2D (TraesCS2D02G172900) were obtained from the EnsemblPlants (https://plants.ensembl.org/Triticum_aestivum/Info/Index), followed by the removal of their transmembrane regions (TMD) to generate a truncated form of the proteins.

AlphaFold2, accessed via the Neurosnap Online Bioinformatics server (https://neurosnap.ai/overview), was utilized for computational 3D structure prediction of native and truncated proteins (Yang et al. 2023). The three-dimensional (3D) structures of myo-inositol hexakisphosphate (InsP□), diphospho-myo-inositol pentakisphosphate (5-InsP□), and bis-diphospho-myo-inositol tetrakisphosphate (1,5-InsP□) were procured from the PubChem database (https://pubchem.ncbi.nlm.nih.gov/) in .SDF format. Molecular docking analyses were executed using CB-Dock2 (https://cadd.labshare.cn/cb-dock2/index.php), identifying favourable binding sites and key interacting residues (Yang et al. 2022). The protein-ligand complexes were further examined using PyMOL v3.0.0, delineating secondary structure elements and polar residues within the binding interface. Protein-ligand interactions were graphically rendered in Adobe Illustrator, accentuating critical residues and summarizing docking insights.

**2.4. Co-immunoprecipitation and Western analysis of interacting proteins**

For co-immunoprecipitation assays, respective yeast cultures were grown in SD medium with appropriate amino acids dropout. Each independent primary yeast culture [containing construct for cMYC-TaVIH2, HA-FLA7, cMYCTaVIH2+HA-FLA7 and Y187 (Wild type), respectively] was grown overnight at 30 ˚C upto an $OD_{600}$ of 1. The secondary culture was incubated for 6 hours, cells were washed and the lysate was prepared using glass beads in buffer (1% SDS, 100 mM NaCl,100 mM Tris-Cl, 1 mM EDTA, 2% Triton and 1mM protease inhibitor (100X Halt protease inhibitor, Thermofisher, U.S.A.). Equal amounts of each lysate was incubated overnight at 4 ˚C with 100% of Protein-G agarose beads and 2 µl of anti-c-MYC antibody. The beads were subsequently washed three times with lysis buffer and centrifuged for 30 sec at 800 x g. 50 µl of loading dye was added to the washed beads and heated at 65 ˚C for 10 min. The elutant was resolved through SDS-PAGE and transferred to the PVDF membrane. Blot was then separated into two parts to detect TaVIH2 and TaFLA7 separately using the respective antibodies. Respective primary antibodies were used for probing (mouse Anti-c-MYC and rabbit anti-HA with 1:2000 dilution). After washing the blots with TBST, they were treated with the secondary antibody (Goat Anti-Mouse IgG (H + L); and Goat Anti-Rabbit IgG (H + L) with 1:5000 dilution. After subsequent washing with TBST, the blot was developed by using BIO-RAD clarity western ECL Substrate.

**2.5. Yeast mating-based split ubiquitin assay**

Split ubiquitin assays were done as described earlier (Obrdlik et al., 2004). The appropriate yeast host strains THY.AP4 and THY.AP5 and gateway cloning-based vectors such as pMetYC gate, pXNgate21-3HA and pXNuB WT gate were used. The TaFLA7 and TaVIH2 templates were PCR amplified using primers containing attB1 and attB2 sites in the forward and reverse primers, respectively. The attB flanking inserts were co-transformed with linearized vectors to the yeast strains using the lithium acetate method for recombination-based invivo cloning. The FLA7 and VIH2 genes were cloned to pMetYC gate and pXNgate 21-3HA vectors, forming C terminal fusions with Cub and NubG, respectively. The Cub vectors and inserts are transformed to haploid THY.AP4 yeast strain and was selected on a synthetic complete medium lacking leucine (SD/-L). Likewise, the Nub vector and inserts are transformed to haploid THY. AP5 yeast strain was selected on a synthetic complete medium lacking tryptophan (SD/-T). The transformed colonies were grown overnight at 28°C in SD media lacking the corresponding dropouts. Subsequently, the cultures were centrifuged and resuspended on a YPDA medium. For interaction studies, mating was performed by mixing an equal amount of the culture, and diploid cells were selected on SD medium lacking the quadruple drop-out of adenine (A), histidine (H), leucine (L), and tryptophan (T). These experiments were repeated three times, and plates were incubated at 28°C for 3-4 days before they were photographed.

**2.6. Localization studies**

TaFLA7 was cloned in pGADT7 vector at EcoR1 and BamH1 sites for the localization experiments. TaVIH2 cDNA was cloned in the pGBKT7 vector using Sma1 and Not1 restriction sites. The constructs were transformed in the Y2H Gold yeast strain and selected on SD-Leu or SD-Trp plates. Yeast spheroplasts were prepared for localization as described earlier (Severance et al., 2004). Mouse monoclonal anti-HA (H.A.:FLA7-pGADT7) : or rabbit Anti-c-Myc (cMYC: VIH2-pGBKT7) primary antibody (Invitrogen, USA) was used for the respective preparations at a ratio of 1:200 followed by 5 washing with blocking buffer. Yeast cells were incubated with Goat Anti-Mouse IgG (H+L) Alexa Flour Plus 488 or Goat Anti-Rabbit IgG (H+L) Alexa Flour Plus 647 (Invitrogen, USA) at a ratio of 1:500 for 4hr at room temperature. Cells were washed with blocking buffer and mounted with Fluor mount (Sigma, USA). Representative fluorescent images were taken using LEICA DM600CS using a 64X oil objective.

**2.7. Luciferase Assay**

Coding sequences (CDS) of TaVIH2 and TaFLA7 were amplified using forward primers containing BamHI and reverse primers containing EcoRI, ensuring that the open reading frame (ORF) remained intact. The amplified products were then cloned into pCAMBIA1300-NLuc and pCAMBIA1300-CLuc vectors. The recombinant plasmids were initially transformed into *E. coli* DH5α cells for propagation and were confirmed by sequencing. Subsequently, the verified plasmids were transformed into the *Agrobacterium tumefaciens* GV3101 strain. Positive clones of GV3101 containing the recombinant plasmids were selected and cultured overnight with appropriate antibiotics. The cells were pelleted and resuspended in freshly prepared induction media containing 10 mM $MgCl_2$, 10 mM MES (pH 5.7), and 150 µM acetosyringone. The optical density (OD) of each culture was adjusted to 0.5, and 1 mL of the Nluc-expressing cells was mixed with 1 mL of the Cluc-expressing cells. The mixture was incubated at 28 °C without shaking for 5–6 hours before agroinfiltration into tobacco leaves (10 µL per spot, with three spots per leaf). The infiltrated plants were maintained in a humidity chamber, kept in the dark for 12 hours, and then exposed to light for 24 hours. Finally, the leaves were harvested, and chemiluminescence was detected, with an exposure time of 20 seconds.

**2.8. Extraction of Inositol Pyrophosphates**

S. cerevisiae cultures were grown at 30 °C in Synthetic complete Dextrose (SD) media until they reached exponential growth, with an $A_{600}$ between 0.6 and 0.8. Cells equivalent to 10 $A_{600}$ units were collected by centrifugation. After washing with ice-cold water, the cells were resuspended in 500 µL of 1 M perchloric acid. The samples were quickly frozen using liquid nitrogen and stored at −80 °C. The samples were briefly vortexed upon thawing, and cell debris was removed by centrifugation at 16,200 g for 5 minutes at 4 °C. The supernatants containing acid-extracted inositol polyphosphates were then purified using titanium dioxide beads (GL Sciences 5020–75000), following the method described by (Wilson and Saiardi 2017). Specifically, the supernatants were combined with 5 mg of $TiO_2$ beads per sample, pre-washed with water and 1 M perchloric acid, followed by incubation on a nutator at 4 °C for 20 minutes. The beads with bound inositol polyphosphates were collected by centrifugation at 5,000 g for 1 minute at 4°C, followed by two washes with 1 M perchloric acid. To elute the inositol polyphosphates, the beads were resuspended twice in 250 µL of 3% ammonium hydroxide, rotated for 5 minutes at 4°C, and then centrifuged at 5,000 g for 1 minute. The combined eluates (totalling 500 µL per sample) were dried using a vacuum centrifuge at room temperature for 5 hours. The dried samples were reconstituted in 20 µL of

water for capillary electrophoresis electrospray ionization mass spectrometry (CE-MS) analysis.

**2.9. CE-MS analysis**

The analyses were conducted as described earlier (Qiu et al. 2020, 2023; Saiardi et al. 2021). An Agilent CE-QQQ system was used for the analysis, which featured an Agilent 7100 capillary electrophoresis unit, an Agilent 6495C Triple Quadrupole mass spectrometer, and an Agilent Jet Stream electrospray ionization source, all connected via an Agilent CE-ESI-MS interface. The sheath liquid, a 50:50 combination of isopropanol and water, was given at a steady flow rate of 10 µL/min using an isocratic Agilent 1200 LC pump and a splitter to ensure exact flow. A 100 cm long fused silica capillary with an internal diameter of 50 µm and an outside diameter of 365 µm was employed to separate the samples. The background electrolyte (BGE) contained 40 mM ammonium acetate that had been adjusted to pH 9.08 with ammonium hydroxide. Before each sample analysis, the capillary was flushed with BGE for 400 seconds. Samples were delivered into the system by applying a pressure of 100 mbar for 15 seconds, resulting in an injection volume of around 30 nL. The MS source settings included a gas temperature of 150 ˚C, flow rate of 11 L/min, nebulizer pressure of 8 psi, and sheath gas temperature of 175˚C. The capillary voltage was set to -2000V, with a nozzle voltage of 2000 V. Furthermore, the negative high-pressure radio frequency (RF) and negative low-pressure RF were kept at 70 and 40 volts, respectively. The multiple reaction monitoring (MRM) parameters were set up as shown in Table 3. The internal standard (IS) stock solution was created using the described method (Qiu et al. 2020; Saiardi et al. 2021). Which was then added to the samples to help with isomer assignment and quantification of InsPs and PP-InsPs. 5 µL of IS was added to 5 µL of the sample and carefully mixed. IPs were quantified by adding known amounts of the matching heavy isotopic references to the samples. After spiking, the final concentrations in the samples were as follows: 4 µM [$^{13}C_6$] 2-OH $InsP_5$, 20 µM [$^{13}C_6$] $InsP_6$, 1 µM [$^{13}C_6$] 5- $InsP_7$, 1 µM [$^{13}C_6$] 1- $InsP_7$, and 1 µM [$^{13}C_6$] 1,5- $InsP_8$. Dorothea Fiedler provided the [13C6] inositol STD (Harmel et al. 2019).

**3. Results**

**3.1 VIH proteins contain variable IDR regions**

Studies in the yeast and mammalian systems have shown that different inositol pyrophosphate kinase function is based on their protein interaction networks (Gokhale 2013;

Rao et al. 2014; Wright and Dyson 2015; Rogers et al. 2021). The human PPIP5K (HsPPIP5K) interaction studies show the typical dual-domains involvement and requirement of the C-terminal intrinsically disordered region (IDR) for interaction (Machkalyan et al. 2016). This HsPPIP5K contains a large C- terminal IDR region (~250-550 aa), a missing characteristic for most plant VIHs (Figure 1& Figure S1). The IDR region was checked in the plant VIH proteins. Our analysis indicated that plant VIH proteins have a variable and lower percentage of IDR representation. The plants VIH show 12-22 % of IDR region (Table 1). Interestingly, wheat TaVIH possesses a higher IDR % when compared to the *Arabidopsis* (Figure 1).

To get insights into the direct and indirect interactions, we performed a String analysis of VIH proteins. Human PPIP5K and yeast (VIP1) analysis yielded a protein-protein network analysis, with nodes indicating the PHO-mediated interactors for VIP and the involvement of HsPPIP5K in other biochemical activities (Figure S2). A similar analysis of wheat VIH2-3B protein shows multifunctional globular proteins, such as actin, as probable interactors. The presence of IDR in the wheat VIH2 and the preliminary String analysis led us to explore its interacting partners.

**3.2 Screening of TaVIH2 interacting partners**

To get molecular insights into the roleof TaVIH2 proteins in stress tolerance, we used yeast two-hybrid (Y2H) cDNA library screen to identify its possible interacting partners. Protein expression of bait (VIH2) in the yeast cells was confirmed by immunoblot analysis (Supplementary Figure S3A). Two pooled wheat cDNA libraries (~4 kb to 300 bp) were prepared for Y2H studies. The smear pattern confirmed the good quality of ds-cDNA (Supplementary Figure S3B). Y2H was performed using TaVIH2-3B as a bait, and this resulted in the identification of 89 putative yeast colonies with a mating efficiency of 3.8 %. Subsequent screening of the colonies led to the identification of ~52 putative interactors (Supplementary Figure S3C&D). Amplicons were generated (Supplementary Figure S4) sequenced, and clones that appeared more than twice were considered for further studies. The analysis led to the shortlisting eleven strong potential interactors with high occurrence in the screening (Table 2). Amongst these interactors, most of the genes encode for cell-wall-related function, including fasciclin-like arabinogalactan protein (FLA), glycosyl-transferases, and glycine-rich structural proteins. The most frequently (nine times) interacting clone was identified as FLA (TraesCS2A02G165600) protein, and further detailed characterization was performed with this protein.

### 3.3 Wheat VIH2 interacts with fasciclin-like arabinogalactan protein (FLA)

To further confirm this interaction, full-length coding sequence of TaFLA7 (1.4 kb) was cloned (TaFLA7:AD+TaVIH2:BD) and co-transformed along with TaVIH2 in the yeast strain. No autoactivation of the TaFLA7 and TaVIH2 was observed in the respective AD and BD vectors (Figure S5A). The yeast co-transformed with TaFLA7 and TaVIH2 showed intense reporter activity (Figure 2A). Next, to further confirm this interaction, yeast colonies were grown on -His/-Leu/-Trp (Auerobasidin) media and the protein extracts were subjected to in vivo pull down assay. For this, first we checked the expression of HA-tagged FLA7 and c-MYC-tagged TaVIH2 in the Y2H Gold yeast strain. Western analysis for both proteins (fused HA:TaFLA7: ~42 kDa) indicated optimal cell expression (Figure 2B left panel). Co-immunoprecipitation was done using an anti-c-MYC antibody. Furthermore, only the TaVIH2 (~110 kDa) was detected in the lysate lacking TaFLA7 (Figure 2B right panel; Lane1), whereas no proteins were detected in wild-type yeast Y187 (Lane3). However, in the pull-down analysis of TaFLA7 and TaVIH2 co-transformed cells, both the TaFLA7 and TaVIH2 proteins were detected by respective tagged antibodies (Figure 2C; Lane 4). These findings suggest that TaVIH2 and TaFLA7 exhibit protein-protein interactions. Next, we also employed spilt ubiquitin-based interaction assays to validate these interactions. The respective plasmids were transformed into the respective haploid yeast strains with appropriate constructs, and mating was performed. The yeast strains were streaked on multiple drop-outs, as indicated in Figure 2C. Our results show that yeast containing only TaFL7 or TaVIH2, and their respective controls (1, 2-haploid yeast; 4 and 5-diploid yeast), exhibit no growth. Further specific interactions were noted in diploid yeast strains harbouring both TaFL7 and TaVIH2-containing constructs (3-diploid yeast), suggesting the protein-protein interactions. To further validate these interactions, we performed a split luciferase complementation assay using tobacco leaf (Nicotiana benthamiana) with the fused protein NLuc-TaFLA7)/CLuc-TaVIH2.

Luciferase complementation imaging (LCI) pair reconstituted luciferase activity in regions where both the fused proteins were expressed compared to controls (Figure 3A). RLU measurement suggested an increase of 7-8 folds of the luminescence activity compared to the controls (Figure 3B). These results confirmed that TaVIH2 may interact with proteins involved in cell-wall maintenance.

### 3.4 VIH2 facilitates the localization of FLA7

Our analysis indicated that TaFLA7 encodes a 367 aa protein (predicted ~40 kDa) containing FAS-like arabinogalactan protein and the presence of a typical transmembrane domain (TMD) with glycophosphatidyl-inositol (GPI) domain (Figure 4A). The protein hydropathy plot also identified a hydrophobic region near the GPI region at the C-terminal (Figure S5B). Next, we studied the localization of the FLA7 protein in yeast cells. Confocal imaging of yeast cells expressing TaFLA7:GFP suggests its presence on the plasma membrane (Figure 4B). Since the wheat FLA7-VIH2 interact and FLA7 is localized to the membrane, we wonder whether VIH2-3B contributes to the localization of FLA7. Previously, we reported that TaVIH2-3B overexpressing lines enhanced the expression of genes involved in cell wall biosynthesis (Shukla et al. 2021). TaVIH2-3B was shown to utilize $InsP_7$ as a substrate likewise to yeast VIP1. Therefore, we tested the localization of FLA7 in different yeast backgrounds. As expected, in the Wild type (WT)( yeast, FLA7 was localized on the plasma membrane but this localisation was affected in the VIP1-defective yeast (Figure 4C). This suggested that localization of the FLA7 was dependent on VIP1 activity. Next, we complemented the yeast vip1Δ mutant and checked for the FLA7 localization. The presence of TaVIH2-3B also restored the localisation of TaFL6 to the plasma membrane in the the yeast vip1Δ strain.

Additionally, we have also profiled the cellular pools of $InsP_6$, 5-$InsP_7$, 1-$InsP_7$, and 1,5-$InsP_8$ with capillary electrophoresis electrospray ionization mass spectrometry (CE-ESI-MS), as described in (Qiu et al. 2020, 2023; Saiardi et al. 2021; Liu et al. 2023; Eisenbeis et al. 2023). This method allows us to investigate the cellular levels of different InsP and PP-InsP species in the yeast transformants. To account for any differences in sample recovery during extraction and $TiO_2$ bead affinity enrichment, the levels of 5-$InsP_7$, 1-$InsP_7$, and 1,5-$InsP_8$ were calculated and plotted in pMol (Figure 5). The observed changes in the 1,5-$InsP_8$ levels (Figure 5) between the WT, vip1Δ mutant and vip1Δ::TaVIH2-3B complemented extracts confirmed that TaVIH2 is a functional $InsP_8$ synthase in yeast and it is likely that the localization of TaFLA7 is dependent of the TaVIH2-derived $InsP_8$. Collectively, our results indicate that TaVIH2-3B interacts with the FLA7 protein and could facilitate its localization to the plasma membrane. Moreover, the differences in 1,5-$InsP_8$ levels witnessed among the WT, *vip1*Δ mutant, and *vip1*Δ mutant complemented with TaVIH2-3B suggest that the appropriate positioning of TaFLA7 could be associated with the activity of the PPIP5K enzyme.

To investigate whether FLA proteins are the possible cellular targets of TaVIH-derived InsP species, we performed in silico docking experiment using the structural model of wheat

FLA7 closest homoeolog viz. TaFLA7-2D and TaFLA7-2A (TraesCS2A02G165600) with various InsP isomers. Notably, the $InsP_6$ was docked robustly at the N-terminal domain of TaFLA7-2A and TaFLA7-2D proteins (Figure 6). Furthermore, docking with 5-$InsP_7$ and 1,5-$InsP_8$, the putative products of TaVIH, revealed that the binding pocket remained unchanged, with key conserved residues contributing to ligand interactions. In TaFLA7-2A, Ser239, Thr256, and His253 were consistently involved in binding all three ligands, whereas in TaFLA7, His228, Ser245, and Asn275 were coordinating with the InsP isomers. This highlights the potential of these FLA proteins to accommodate diverse inositol phosphate ligands. Additionally, truncated versions of the proteins, lacking the transmembrane (TMD) domain, retained identical binding pockets and conserved residues, indicating that the TMD does not influence ligand binding (Figure S6). These findings support the structural and functional integrity of the ligand-binding domain in TaFLA7, independent of the TMD.

### 3.5. FLA7 is differentially expressed in wheat tissue

The FLA proteins are known to respond to different stress conditions and are involved in plant growth and development (Zang et al. 2015; Cagnola et al. 2018; Wu et al. 2020; Ma et al. 2022; Yao et al. 2023). These observations suggest that VIH2 and its interacting partners could participate in similar pathways. To further characterize the wheat FLA7, we studied its expression in different tissues and under various stress conditions. The *TaFLA7* was expressed in the grain at the Zadoks scale (Z) 71 stage (watery ripe with the start of grain filling) and in the spike at Z65 (50% of the spikes had yellow anthers) of wheat development (Figure S7A). The transcript expression of *TaFLA7* showed significant upregulation in the shoot tissue when subjected to drought stress after 1 hr and 6 hrs (Figure S7B). Our quantitative RT-PCR results suggested a significant upregulation in the shoot or root tissue subjected to drought stress (Figure S7C). Quantitative RT-PCR showed a high expression of *TaFLA7* towards 28 days after the anthesis (DAA) stages of grain development (Figure S7D). Expression analysis of *TaFLA7* in different wheat grain tissue using the eFP wheat browser revealed its high expression in embryo and aleurone layers of the grain (Figure S8). The tissue-specific eFP wheat browser analysis indicates the high expression of *TaFLA7* in grains, shoot axis, and spikelets (Figure S9). Altogether, the expression data of the *TaFLA7* show transcriptional changes during desiccation, a prerequisite step in grain maturation.

## 4. Discussion

Protein-protein interaction networks provide valuable insights into biological processes and complex metabolic functions within living cells. The Y2H system leverages eukaryotic transcriptional activators with distinct functional domains for DNA-binding and transactivation, making it a powerful and rapid approach to discovering new protein interactions (He et al. 2019). In this study, a high-quality cDNA library using RNA extracted from wheat seedlings was constructed. Our work identified several interactors of TaVIH2 proteins, which serve as promising entry points for further exploration of their regulatory network in the developmental process. Recently, it was demonstrated that the Triticum aestivum (hexaploid wheat) genome encodes functional PPIP5K isoforms, identified as TaVIH2-3B (Shukla et al. 2021). Moreover, the heterologous expression of wheat TaVIH2-3B in Arabidopsis imparts drought tolerance. These Arabidopsis transgenic lines expressing TaVIH2 also exhibit a reprogramming of gene expression involved in cell-wall metabolism and stress response pathways (Shukla et al. 2021). In particular differential expression of genes linked to ABA biosynthesis, cell wall maintenance, and cytochrome P-450 monooxygenases were highly upregulated. Although the level of InsPs seems to be important in imparting such a function, it remains to be studied if plant PP-InsP synthase, such as VIH at the protein level, could be involved directly.

Multi-protein interactions were more accessible by IDRs, which helped them connect with other proteins in the cell. Abelson (Abl), a protein non-receptor tyrosine kinase, has an IDR domain (around 900 amino acids) that has been implicated in a variety of tasks in Drosophila, including the regulation of cell shape and cytoskeleton development (Rogers et al. 2021). Similarly, the human PPIP5K domains' association with proteins involved in actin cytoskeleton structure and phosphatidylinositol biosynthesis was attributed to the IDR's existence (Machkalyan et al. 2016). The interaction studies were pursued using human PPIP5K (HsPPIP5K) (Machkalyan et al. 2016). Human PPIP5K, besides containing the typical dual-domain, also possesses a C-terminal IDR (Machkalyan et al. 2016). This IDR in HsPPIP5K spans a large portion (~250-550 amino acids), a feature that is not very common in most plant VIHs (Figure S1). IDRs assist in their interaction with multiple proteins to facilitate their cellular activities (Ward et al. 2004).

Although VIH proteins have been identified in several plants (Laha et al. 2015; Zhu et al. 2019), including wheat (Shukla et al. 2021), the IDR domains are relatively smaller, ranging from approximately 33-56 amino acids, and their functional roles remain to be elucidated. Our network analysis using the String database can provide clues for the regulatory network of the VIH proteins (Figure S2). Human PPIP5K and yeast (VIP1)

analysis resulted in the protein-protein network analysis with nodes pointing towards the PHO-mediated interactors for the VIP and involvement of HsPPIP5K in other biochemical activities (Figure S2). A similar analysis of wheat VIH shows a network with cytoskeletal actin as a probable interactor. Actin is involved in forming microfilaments in the cytoskeleton and can modulate the cellular shape (Pollard and Cooper 2009). This study identified multiple interactors of VIH2, yet most of them are speculated to be involved in cell wall maintenance. The speculative parallels of VIP1 in yeast and VIH in lets us postulate that plant VIH is likely involved in cell wall cementing and homeostasis. The conserved role of VIH was demonstrated in the important cellular function of Pi-homeostasis (Dong et al. 2019; Zhu et al. 2019; Riemer et al. 2021). Under nutrient-limiting conditions, VIP1 and its ortholog in Schizosaccharomyces pombe (Asp1) kinase were shown to control physiological changes such as dimorphic switch, cell-to-cell, cell-substrate adhesion and unipolar budding (Pöhlmann and Fleig 2010). The ability of TaVIH2 to facilitate the localization of TaFLA7 (Figure 4) provides new insight into the functioning of VIH proteins. Based on our observations and previous reports, the involvement of VIH proteins points towards their role in modulating the cellular boundaries and shape (Figure 7). Such phenotypic changes, including the formation of pseudo-hyphal filaments in yeast (Norman et al. 2018), help sustain themselves under stress conditions, yet their similar involvement in plants needs more investigation. Previous biochemical investigations of TaVIH2-3B overexpressing lines in Arabidopsis indicated changes in cell wall cementing metabolites such as cellulose, arabino-xylan, and arabino-galactan (Shukla et al. 2021). Furthermore, RNAseq analysis of the Col-0 and TaVIH2 overexpressing lines suggested high expression of genes involved in cell wall biosynthesis (Shukla et al. 2021). Together with these results, our findings suggest that VIH2 can regulate the composition of cell wall cementing pathways by localizing the involved proteins to their correct positions. The intriguing role of VIH protein overexpression in modulating cell wall composition requires further investigation. Specifically, the in-vivo levels of $InsP_7$/$InsP_8$ (Figure 5) confirm that the PPIP5K enzymatic activity previously demonstrated with the purified TaVIH2-3B kinase (Shukla et al., 2021) is also functionally active in yeast cells. Therefore, either the synthesis of $InsP_8$ or the presence of TaVIH2-3B protein in the yeast cell are directly influencing the correct localization of the TaFLA7 to the plasma membrane. These measurements therefore validate that TaVIH2-3B maintains its PPIP5K activity in vivo, as evidenced by its ability to modulate $InsP_7$/$InsP_8$ levels in a heterologous yeast system. This, in turn, supports its proposed role in regulating interacting partners such as TaFLA7.

Furthermore, it is crucial to investigate how this localization occurs and to identify which region of TaFLA7 interacts with TaVIH2-3B and understanding the role in such interaction may also be critical for future study. In the aftermath of the current study, it will be interesting to check if $InsP_7$/$InsP_8$ could modulate the protein-protein interactions of transcription factors that are primarily involved in water-deficient stress conditions. Although as primary evidence, our docking study provides insight into the ability of InsPx to bind specific regions of FLA7 (Figure S6). This study remains to be further investigated so as to unravel the new mechanistic insights into drought tolerance that could be mediated by cell wall maintenance. Studies using Arabidopsis have deciphered multiple roles of VIHs in different biological processes. However, such efforts should be expanded to crop plants such as wheat for translational research.

**Acknowledgements**

The authors thank the Executive Director for the facilities and support. This study was supported by the Department of Biotechnology, Basic Plant Biology Grant to AKP [BT/PR12432/BPA/118/35/2014]. Part of this work was also supported by the NABI-CORE grant to A.K.P. and by the Deutsche Forschungsgemeinschaft (DFG) under Germany's Excellence Strategy CIBSS, EXC-2189, Project ID 390939984 to H.J. DBT-eLibrary Consortium (DeLCON) is acknowledged for providing timely support and access to e-resources for this work. A.S. acknowledges Centre For Integrative Biological Signalling Studies for PostDoctral Fellowship. D. L. acknowledges the Department of Biotechnology (DBT) for HGK-Innovative Young Biotechnologist Award (BT/13/IYBA/2020/04). We thank Dr. Santosh Satbhai (IISER-M) for sharing reagents for Yeast mating-based Split Ubiquitin Assay.

**Declarations**

**Conflict of interest**

The authors declare that they have no known competing financial interests or personal relationships that could have appeared to influence the work reported in this manuscript.

**Data Availability**

No new datasets were generated during the current study.

**Figures for the legends:**

**Figure 1: In-silico calculation of the Intrinsic Disorder Regions (IDR) of VIH and PPIP5K proteins.** IDR was calculated based on the (Mizianty et al. 2010; Walsh et al. 2012; Han et al. 2023) along with the percentage region score of the mentioned proteins.

**Figure 2: Interaction of TaVIH2-3B with TaFLA7 as identified during Y2H screening.** (A) Y2H assay using full-length TaFLA7 and VIH2 as represented by GAL plates containing -L-T and without GAL plates containing -HLT. (C) Western analysis of the wheat FLA7 in the yeast strains harbouring independent clones Lane1: cMYC-TaVIH2; Lane2: HA-TaFLA7; Lane3: Wildtype Y187; Lane4: cotransformed clones of cMYC-TaVIH2+HA-TaFLA7. The numbers indicated the expected molecular weight of the detected proteins. (B) Split-ubiquitin yeast two-hybrid interaction assay of the TaFLA7 and TaVIH2. The appropriate colonies were streaked on single dropout media SD-T (for monokaryon yeast strain with pMETYC:TaVIH2), SD-L for (monokaryon yeast strain pXNgate221:TaFLA7) and double dropout (-LT for dikaryon) and for interactors using quadruple dropout (-AHLT).

**Figure 3: Luciferase reporter assay to characterization of TaFLA7 interaction with VIH2.** (A) Luciferase assay of TaFLA7 with VIH2 using tobacco leaves. (B) RLU measurement for the strength of interaction. The values shown are the mean ± SE; n = 4. Student's t test was performed (*$p < 0.001$).

**Figure 4: The localization of TaFLA7 in ScVIP1 mutant.** (A) Schematic representation of the TaFLA7 protein domain architecture. The N-terminal signal peptide and conserved cysteine-rich (CS) motif are shown in red. The central Fas-like arabinogalactan domain is highlighted in blue, followed by a predicted transmembrane domain (TMD) in yellow. The C-terminal region includes GPI-anchor attachment sites (Ω^1 and Ω^2) predicted by big-PI Plant Predictor. Amino acid positions for each domain are indicated. (B) In situ localization of the TaFLA7 in wild-type and vip1Δ yeast strains. Constructs were introduced under pYES2 vector with or without TaVIH2-3B. HA-tagged TaFLA7 was detected by immunofluorescence. In vip1Δ cells, co-expression with TaVIH2-3B led to increased plasma membrane enrichment of TaFLA7. Right panel: higher magnification images showing plasma membrane enrichment in wild-type and vip1Δ cells. Scale bars are indicated for each panel. Fluorescence was measured using a Zeiss fluorescence microscope (Axio Imager Z2) with an Axiocam MRm camera at 63X. Representative images are shown and similar observations were noted for 3-4 independent transformed colonies of yeast.

**Figure 5: Quantification of inositol pyrophosphate levels using CE-ESI-MS.** The inositol pyrophosphate levels in extracts of the WT + pYES2 , vip1Δ + pYES2, and vip1Δ + TaVIH2-3B strains that were transformed with TaFLA7 are displayed for 1,5-$InsP_8$, 5-$InsP_7$, and 1-

$InsP_7$. The values shown are the mean ± SE; n = 5. Student's t test was performed (*p < 0.001).

**Figure 6: Molecular docking of TaFLA7 homoeologs (TaFLA7-2A & 2D) with $InsP_6$, 5-$InsP_7$, and 1,5-$InsP_8$.** Schematic representation of (A) TaFLA7-2A and (B) TaFLA7-2D structures, highlighting the transmembrane domain (TMD) and ligand-binding site. Docked conformations of $InsP_6$, 5-$InsP_7$, and 1,5-$InsP_8$ are shown with key interacting residues labelled. Ligands (green sticks) form polar bonds (yellow dashed lines), revealing distinct binding orientations and interaction patterns.

**Figure 7: Schematic representation drawing parallels for the possible function of VIH proteins in multiple cellular processes**. In yeast, VIP proteins and their products were shown to be involved in the cell boundary rearrangements, including regulation of microtubule rearrangement and filamentous growth of the fungi under nutrient-limiting conditions (Pöhlmann and Fleig 2010; Pöhlmann et al. 2014). Plant VIHs are known to be involved in phosphate (Pi) homeostasis and plant defence (Laha et al. 2015; Dong et al. 2019; Riemer et al. 2021). Recently, the role of plant VIH in cell wall-related rearrangements has been established (Shukla et al. 2021). The participation of genes encoding VIP1/VIH proteins in cell wall rearrangement in both yeast and plants could reflect the conserved function of the proteins across species (Pöhlmann et al. 2014; Shukla et al. 2021).

**Table 1: Intrinsic disorder region (IDR) percentage, length and disorder segment position in the human (*Homo sapiens*) and plant (*Arabidospsi thaliana*, At; *Oryza sativa*, Os; *Triticum aestivum*, wheat) encoded PPIP5K-like proteins. Efficient disorder prediction was made using ESpritz (version 1.3).**

| Name | % Disorder | Length of largest segment | Disorder segment position( in AA) | Total AA |
|---|---|---|---|---|
| HsPPIP5K1 | 29.58 | 167 | 1107 to 1274 | 1433 |
| HsPPIP5K2 | 29.92 | 155 | 873 to 1028 | 1243 |
| AtVIH1 | 13.34 | 65 | 792 to 857 | 1049 |
| AtVIH2 | 12.40 | 69 | 797 to 866 | 1056 |
| OsVIH1 | 16.47 | 81 | 786 to 867 | 1043 |
| OsVIH2 | 10.54 | 30 | 648 to 678 | 758 |
| TaVIH2-3B | 12.93 | 37 | 815 to 837 | 1036 |
| TaVIH1-4D | 13.65 | 56 | 797 to 853 | 1047 |

**Table 2: Interacting partners of wheat VIH2 proteins.** The tables indicate the gene IDs with their annotated function based on homology. The numbers indicate the frequency of the occurrence of the clone as an interacting partner from the library.

| S.No | Gene Function | Known functional in Planta | New TRIAE_ ID | Number of Occurrences |
|---|---|---|---|---|
| 1. | **Fasciclin-like protein FLA7-2D** | Cell wall biosynthesis, stress response, | TraesCS2D02G172900.1 | 9 |
| 2. | **Glycosyl-transferases (GT1)** | Cell wall biosynthesis, stress response, cell wall cementing, transfer sugar moieties | TraesCS6B02G339100.1 | 6 |
| 3. | **Xylan arabinosyl transferase (Xat1)** | Cell wall biosynthesis, stress response, cell wall cementing | TraesCS6A02G309400.1 | 5 |
| 4. | **Glycine-rich cell wall structural protein-like** | Cell wall biosynthesis, stress response | TraesCS2B02G541900 | 5 |
| 5. | **NADH-ubiquinone reductase complex 1 MLRQ subunit;** | Uncharacterized protein | TraesCS7A02G238600 | 3 |
| 6. | **Hypothetical protein TRIUR3_12806** | Auxin efflux transporter that acts as a negative regulator of light signalling to promote hypocotyl elongation | TraesCS4A02G016700 | 3 |
| 7. | **ABC transporter B family member** | Metal transporter involved in the sequestration of aluminium into vacuoles | TraesCS5A02G392600 | 4 |
| 8. | **Short-chain dehydrogenase reductase** | Glucose signalling and abscisic acid biosynthesis and functions | TraesCS2B02G116700 | 3 |

| | | | | |
|---|---|---|---|---|
| 9. | **Ethylene-responsive element binding protein 1 (EREB1)** | Increases tolerance to abiotic stress | TraesCS7B02G062200 | 4 |
| 10 | **W.W. domain-binding protein (containing PPG PPP motif)** | Modules mediate protein-protein interactions by recognizing proline-rich peptide motifs and phosphorylated serine/threonine-proline sites. | TraesCS7B02G062200 | 3 |

**Table 3: MS parameters for MRM transitions**

| Molecular name | Precursor Ion | Product Ion | Collision Energy (V) | Cell Accelerator Voltage |
|---|---|---|---|---|
| [$^{13}C_6$] $InsP_5$ | 292 | 504.9 | 9 | 3 |
| $InsP_5$ | 289 | 498.9 | 9 | 3 |
| [$^{13}C_6$] $InsP_6$ | 331.9 | 79.1 | 53 | 4 |
| $InsP_6$ | 328.9 | 79.1 | 53 | 4 |
| [$^{13}C_6$] $InsP_7$ | 371.9 | 322.9 | 9 | 3 |
| [$^{18}O_2$] 4-$InsP_7$ | 370.9 | 319.9 | 9 | 3 |
| $InsP_7$ | 368.9 | 319.9 | 9 | 3 |
| 1,5[$^{13}C_6$] $InsP_8$ | 411.9 | 362.8 | 9 | 1 |
| 1,5$InsP_8$ | 408.9 | 359.8 | 9 | 1 |

Polarity: Negative, Dwell: 80, Fragmentor (V): 166

**Reference:**


Azevedo C, Burton A, Ruiz-Mateos E, et al (2009) Inositol pyrophosphate mediated pyrophosphorylation of AP3B1 regulates HIV-1 Gag release. Proc Natl Acad Sci 106:21161–21166. https://doi.org/10.1073/pnas.0909176106

Bhandari R, Hamid A, Ladke JS, et al (2024) Interaction with IP6K1 supports pyrophosphorylation of substrate proteins by the inositol pyrophosphate 5-InsP7. Biosci Rep BSR20240792. https://doi.org/10.1042/BSR20240792

Cagnola JI, Dumont de Chassart GJ, Ibarra SE, et al (2018) Reduced expression of selected FASCICLIN-LIKE ARABINOGALACTAN PROTEIN genes associates with the abortion of kernels in field crops of Zea mays (maize) and of Arabidopsis seeds. Plant Cell Environ 41:661–674. https://doi.org/https://doi.org/10.1111/pce.13136

Chabert V, Kim G-D, Qiu D, et al (2023) Inositol pyrophosphate dynamics reveals control of the yeast phosphate starvation  program through 1,5-IP(8) and the SPX domain of Pho81. Elife 12:. https://doi.org/10.7554/eLife.87956

Choi JH, Williams J, Cho J, et al., (2007) Purification, sequencing, and molecular identification of a mammalian PP-InsP5 kinase that is activated when cells are exposed to hyperosmotic stress. J. Biol. Chem 282 (42): 30763-30775 doi: 10.1074/jbc.M704655200

Desai M, Rangarajan P, Donahue JL, et al (2014) Two inositol hexakisphosphate kinases drive inositol pyrophosphate synthesis in plants. Plant J 80:642–653. https://doi.org/10.1111/tpj.12669

Dong J, Ma G, Sui L, et al (2019) Inositol Pyrophosphate InsP8 Acts as an Intracellular Phosphate Signal in Arabidopsis. Mol Plant 12:1463–1473. https://doi.org/10.1016/j.molp.2019.08.002

Eisenbeis VB, Qiu D, Gorka O, et al (2023) β-lapachone regulates mammalian inositol pyrophosphate levels in an NQO1- and oxygen-dependent manner. Proc Natl Acad Sci 120:e2306868120. https://doi.org/10.1073/pnas.2306868120

Fridy PC, Otto JC, Dollins DE, York JD (2007) Cloning and Characterization of Two Human VIP1-like Inositol Hexakisphosphate and Diphosphoinositol Pentakisphosphate Kinases. J Biol Chem 282:30754–30762. https://doi.org/10.1074/jbc.m704656200

Gokhale NA (2013) Membrane phosphoinositides and protein–membrane interactions. Amino Acids 45:751–754. https://doi.org/10.1007/s00726-013-1512-2

Han B, Ren C, Wang W, et al (2023) Computational Prediction of Protein Intrinsically Disordered Region Related  Interactions and Functions. Genes (Basel) 14:. https://doi.org/10.3390/genes14020432

Harmel RK, Puschmann R, Nguyen Trung M, et al (2019) Harnessing (13)C-labeled myo-inositol to interrogate inositol phosphate messengers by NMR. Chem Sci 10:5267–5274. https://doi.org/10.1039/c9sc00151d

He Y, Wu L, Liu X, et al (2019) Yeast two-hybrid screening for proteins that interact with PFT in wheat. Sci Rep 9:15521. https://doi.org/10.1038/s41598-019-52030-x

Jung J-Y, Ried MK, Hothorn M, Poirier Y (2018) Control of plant phosphate homeostasis by

inositol pyrophosphates and the SPX domain. Curr Opin Biotechnol 49:156–162. https://doi.org/https://doi.org/10.1016/j.copbio.2017.08.012

Laha D, Johnen P, Azevedo C, et al (2015) VIH2 Regulates the Synthesis of Inositol Pyrophosphate InsP8 and Jasmonate-Dependent Defenses in Arabidopsis. Plant Cell 27:1082–1097. https://doi.org/10.1105/tpc.114.135160

Laha D, Parvin N, Dynowski M, et al (2016) Inositol Polyphosphate Binding Specificity of the Jasmonate Receptor Complex . Plant Physiol 171:2364–2370. https://doi.org/10.1104/pp.16.00694

Laha NP, Giehl RFH, Riemer E, et al (2022) INOSITOL (1,3,4) TRIPHOSPHATE 5/6 KINASE1-dependent inositol polyphosphates regulate auxin responses in Arabidopsis. Plant Physiol 190:2722–2738. https://doi.org/10.1093/plphys/kiac425

Land ES, Cridland CA, Craige B, et al (2021) A Role for Inositol Pyrophosphates in the Metabolic Adaptations to Low Phosphate in Arabidopsis. Metabolites 11:. https://doi.org/10.3390/metabo11090601

Lee Y-S, Mulugu S, York JD, O'Shea EK (2007) Regulation of a cyclin-CDK-CDK inhibitor complex by inositol pyrophosphates. Science 316:109–112. https://doi.org/10.1126/science.1139080

Liu G, Riemer E, Schneider R, et al (2023) The phytase RipBL1 enables the assignment of a specific inositol phosphate isomer as a structural component of human kidney stones. RSC Chem Biol 4:300–309. https://doi.org/10.1039/d2cb00235c

Livak KJ, Schmittgen TD (2001) Analysis of Relative Gene Expression Data Using Real-Time Quantitative PCR and the 2−ΔΔCT Method. Methods 25:402–408. https://doi.org/10.1006/meth.2001.1262

Ma Y, MacMillan CP, de Vries L, et al (2022) FLA11 and FLA12 glycoproteins fine-tune stem secondary wall properties in response to mechanical stresses. New Phytol 233:1750–1767. https://doi.org/10.1111/nph.17898

Machkalyan G, Trieu P, Pétrin D, et al (2016) PPIP5K1 interacts with the exocyst complex through a C-terminal intrinsically disordered domain and regulates cell motility. Cell Signal 28:. https://doi.org/10.1016/j.cellsig.2016.02.002

Meena V, Kaur G, Joon R, et al (2024) Transcriptome and biochemical analysis in hexaploid wheat with contrasting tolerance to iron deficiency pinpoints multi-layered molecular process. Plant Physiol Biochem 207:108336. https://doi.org/https://doi.org/10.1016/j.plaphy.2024.108336

Mizianty MJ, Stach W, Chen K, et al (2010) Improved sequence-based prediction of

disordered regions with multilayer fusion of multiple information sources. Bioinformatics 26:i489–i496. https://doi.org/10.1093/bioinformatics/btq373

Mulugu S, Bai W, Fridy P, et al (2007) A Conserved Family of Enzymes That Phosphorylate Inositol Hexakisphosphate. Science 316:106–109. https://doi.org/10.1126/science.1139099

Norman KL, Shively CA, De La Rocha AJ, et al (2018) Inositol polyphosphates regulate and predict yeast pseudohyphal growth phenotypes. PLoS Genet 14:e1007493–e1007493. https://doi.org/10.1371/journal.pgen.1007493

Obrdlik P, El-Bakkoury M, Hamacher T, Cappellaro C, Vilarino C, Fleischer C, Ellerbrok H, Kamuzinzi R, Ledent V, Blaudez D, Sanders D, Revuelta JL, Boles E, Andre B, Frommer WB Proc Natl Acad Sci U S A. 2004 Aug 17;101(33):12242-7.

Pipercevic J, Kohl B, Gerasimaite R, et al (2023) Inositol pyrophosphates activate the vacuolar transport chaperone complex in yeast by disrupting a homotypic SPX domain interaction. Nat Commun 14:2645. https://doi.org/10.1038/s41467-023-38315-w

Pöhlmann J, Fleig U (2010) Asp1, a Conserved 1/3 Inositol Polyphosphate Kinase, Regulates the Dimorphic Switch in Schizosaccharomyces pombe. Mol Cell Biol 30:4535. https://doi.org/10.1128/MCB.00472-10

Pöhlmann J, Risse C, Seidel C, et al (2014) The Vip1 inositol polyphosphate kinase family regulates polarized growth and modulates the microtubule cytoskeleton in fungi. PLoS Genet 10:e1004586–e1004586. https://doi.org/10.1371/journal.pgen.1004586

Pollard TD, Cooper JA (2009) Actin, a central player in cell shape and movement. Science 326:1208–1212. https://doi.org/10.1126/science.1175862

Qiu D, Gu C, Liu G, et al (2023) Capillary electrophoresis mass spectrometry identifies new isomers of inositol  pyrophosphates in mammalian tissues. Chem Sci 14:658–667. https://doi.org/10.1039/d2sc05147h

Qiu D, Wilson MS, Eisenbeis VB, et al (2020) Analysis of inositol phosphate metabolism by capillary electrophoresis electrospray ionization mass spectrometry. Nat Commun 11:6035. https://doi.org/10.1038/s41467-020-19928-x

Ramírez-González RH, Borrill P, Lang D, et al (2018) The transcriptional landscape of polyploid wheat. Science 361:. https://doi.org/10.1126/science.aar6089

Rao F, Cha J, Xu J, et al (2014) Inositol pyrophosphates mediate the DNA-PK/ATM-p53 cell death pathway by regulating CK2 phosphorylation of Tti1/Tel2. Mol Cell 54:119–132. https://doi.org/10.1016/j.molcel.2014.02.020

Ried MK, Wild R, Zhu J, et al (2021) Inositol pyrophosphates promote the interaction of SPX

domains with the coiled-coil motif of PHR transcription factors to regulate plant phosphate homeostasis. Nat Commun 12:384. https://doi.org/10.1038/s41467-020-20681-4

Riemer E, Qiu D, Laha D, et al (2021) ITPK1 is an InsP6/ADP phosphotransferase that controls phosphate signaling in Arabidopsis. Mol Plant 14:1864–1880. https://doi.org/https://doi.org/10.1016/j.molp.2021.07.011

Rogers EM, Allred SC, Peifer M (2021) Abelson kinase's intrinsically disordered region plays essential roles in protein function and protein stability. Cell Commun Signal 19:27. https://doi.org/10.1186/s12964-020-00703-w

Saiardi A (2004) Phosphorylation of Proteins by Inositol Pyrophosphates. Science (80- ) 306:2101–2105. https://doi.org/10.1126/science.1103344

Saiardi A, Qiu D, Eisenbeis VB, Jessen HJ (2021) Absolute Quantitation of Inositol Pyrophosphates by Capillary Electrophoresis Electrospray Ionization Mass Spectrometry. JoVE e62847. https://doi.org/doi:10.3791/62847

Sanchez AM, Garg A, Shuman S, Schwer B (2019) Inositol pyrophosphates impact phosphate homeostasis via modulation of RNA 3' processing and transcription termination. Nucleic Acids Res 47:8452–8469. https://doi.org/10.1093/nar/gkz567

Shears SB (2015) Inositol pyrophosphates: why so many phosphates? Adv Biol Regul 57:203–216. https://doi.org/10.1016/j.jbior.2014.09.015

Shukla A, Kaur M, Kanwar S, et al (2021) Wheat inositol pyrophosphate kinase TaVIH2-3B modulates cell-wall composition and drought tolerance in Arabidopsis. BMC Biol 19:261. https://doi.org/10.1186/s12915-021-01198-8

Szijgyarto Z, Garedew A, Azevedo C, et al (2011) Influence of inositol pyrophosphates on cellular energy dynamics. Science 334(6057):802-5 DOI: 10.1126/science.1211908

Szklarczyk D, Kirsch R, Koutrouli M, et al (2023) The STRING database in 2023: protein-protein association networks and functional enrichment analyses for any sequenced genome of interest. Nucleic Acids Res 51:D638–D646. https://doi.org/10.1093/nar/gkac1000

Thota SG, Bhandari R (2015) The emerging roles of inositol pyrophosphates in eukaryotic cell physiology. J Biosci 40:593–605. https://doi.org/10.1007/s12038-015-9549-x

Walsh I, Martin AJM, Di Domenico T, Tosatto SCE (2012) ESpritz: accurate and fast prediction of protein disorder. Bioinformatics 28:503–509. https://doi.org/10.1093/bioinformatics/btr682

Ward JJ, Sodhi JS, McGuffin LJ, et al (2004) Prediction and Functional Analysis of Native

Disorder in Proteins from the Three Kingdoms of Life. J Mol Biol 337:635–645. https://doi.org/https://doi.org/10.1016/j.jmb.2004.02.002

Wilson MSC, Saiardi A (2017) Importance of Radioactive Labelling to Elucidate Inositol Polyphosphate Signalling. Top Curr Chem 375:14. https://doi.org/10.1007/s41061-016-0099-y

Wright PE, Dyson HJ (2015) Intrinsically disordered proteins in cellular signalling and regulation. Nat Rev Mol Cell Biol 16:18–29. https://doi.org/10.1038/nrm3920

Wu X, Lai Y, Lv L, et al (2020) Fasciclin-like arabinogalactan gene family in Nicotiana benthamiana: genome-wide identification, classification and expression in response to pathogens. BMC Plant Biol 20:305. https://doi.org/10.1186/s12870-020-02501-5

Yao K, Yao Y, Ding Z, et al (2023) Characterization of the FLA Gene Family in Tomato (Solanum lycopersicum L.) and the Expression Analysis of SlFLAs in Response to Hormone and Abiotic Stresses. Int J Mol Sci 24:. https://doi.org/10.3390/ijms242216063

Yang Liu, Xiaocong Yang, Jianhong Gan, Shuang Chen, Zhi-Xiong Xiao, Yang Cao, CB-Dock2: improved protein–ligand blind docking by integrating cavity detection, docking and homologous template fitting, Nucleic Acids Research, Volume 50, Issue W1, 5 July 2022, Pages W159–W164. https://doi.org/10.1093/nar/gkac394

Yang, Z., Zeng, X., Zhao, Y. and Chen, R., 2023. AlphaFold2 and its applications in the fields of biology and medicine. Signal Transduction and Targeted Therapy, 8(1), p.115. https://doi.org/10.1038/s41392-023-01381-z

Zang L, Zheng T, Chu Y, et al (2015) Genome-Wide Analysis of the Fasciclin-Like Arabinogalactan Protein Gene Family Reveals Differential Expression Patterns, Localization, and Salt Stress Response in Populus . Front. Plant Sci. 6

Zhou J, Hu Q, Xiao X, et al (2021) Mechanism of phosphate sensing and signaling revealed by rice SPX1-PHR2 complex structure. Nat Commun 12:7040. https://doi.org/10.1038/s41467-021-27391-5

Zhu J, Lau K, Puschmann R, et al (2019) Two bifunctional inositol pyrophosphate kinases/phosphatases control plant phosphate homeostasis. Elife 8:e43582. https://doi.org/10.7554/eLife.43582

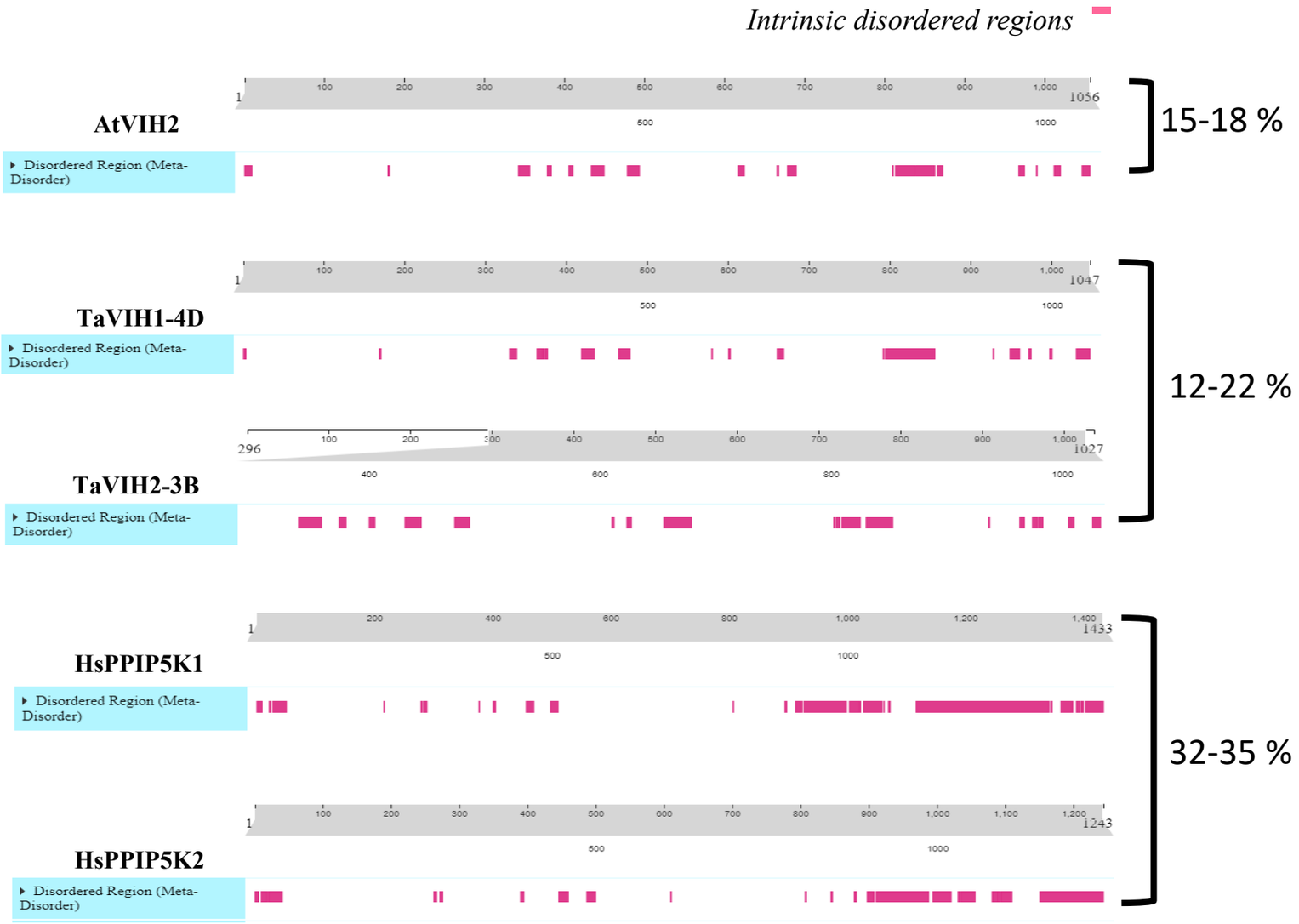
Intrinsic disordered regions
AtVIH2
Disordered Region (Meta-Disorder)
15-18 %
TaVIH1-4D
Disordered Region (Meta-Disorder)
TaVIH2-3B
Disordered Region (Meta-Disorder)
12-22 %
HsPPIP5K1
Disordered Region (Meta-Disorder)
HsPPIP5K2
Disordered Region (Meta-Disorder)
32-35 %

Figure 1

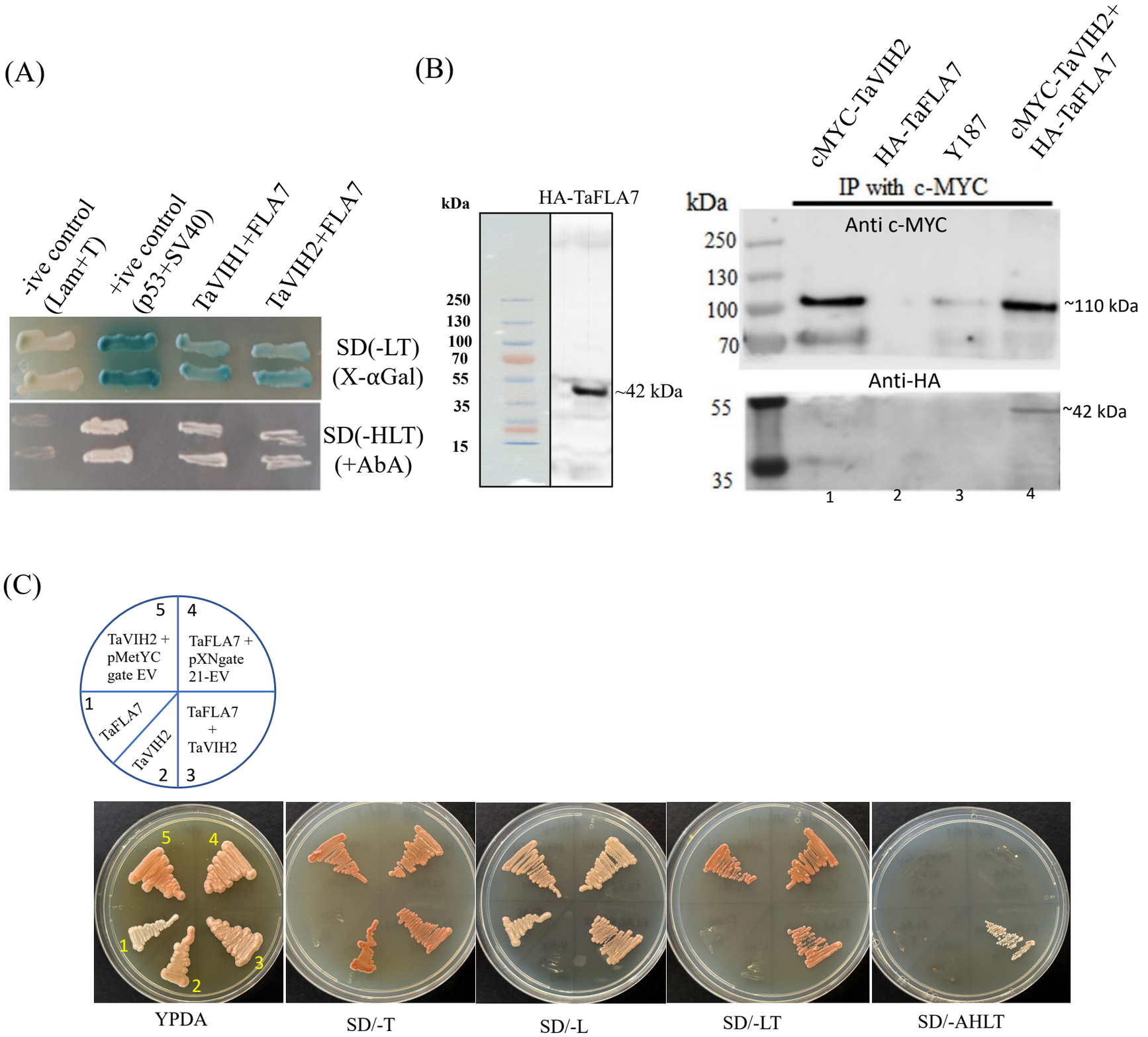
(A)
-ive control (Lam+T)
+ive control (p53+SV40)
TaVIH1+FLA7
TaVIH2+FLA7
SD(-LT) (X-αGal)
SD(-HLT) (+AbA)
(B)
kDa
HA-TaFLA7
250
130
100
70
55
35
15
~42 kDa
cMYC-TaVIH2
HA-TaFLA7
Y187
cMYC-TaVIH2+ HA-TaFLA7
IP with c-MYC
kDa
Anti c-MYC
250
130
100
70
~110 kDa
Anti-HA
55
35
~42 kDa
1
2
3
4
(C)
5
4
TaVIH2 + pMetYC gate EV
TaFLA7 + pXNgate 21-EV
1
TaFLA7
TaVIH2
TaFLA7 + TaVIH2
2
3
YPDA
SD/-T
SD/-L
SD/-LT
SD/-AHLT

Figure 2

(A)

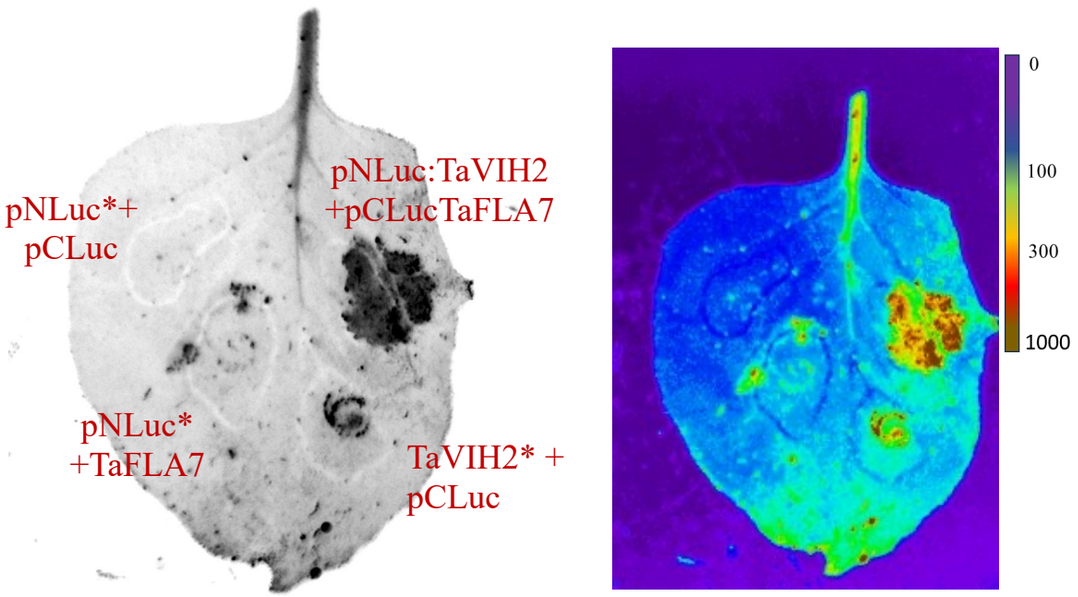
pNLuc*+
pCLuc
pNLuc:TaVIH2
+pCLucTaFLA7
pNLuc*
+TaFLA7
TaVIH2* +
pCLuc
0
100
300
1000

(B)

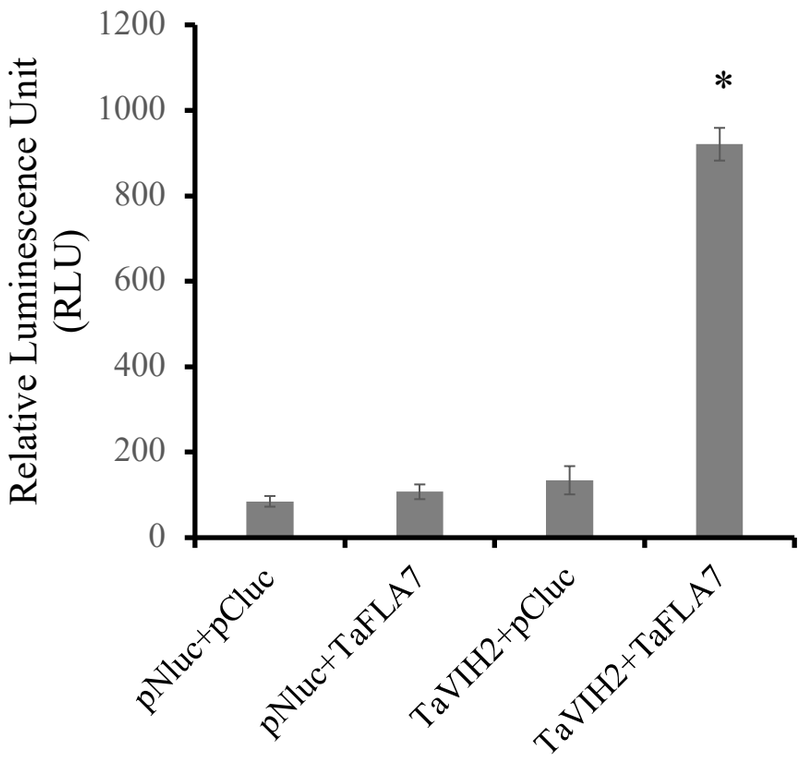
Relative Luminescence Unit
(RLU)
1200
1000
800
600
400
200
0
*
pNluc+pCluc
pNluc+TaFLA7
TaVIH2+pCluc
TaVIH2+TaFLA7

Figure 3

(A)

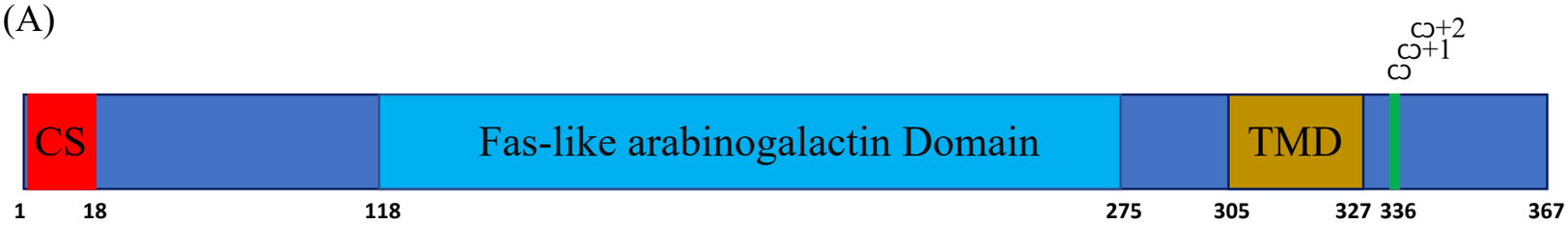
ω
ω+1
ω+2
CS
Fas-like arabinogalactin Domain
TMD
1
18
118
275
305
327
336
367

(B)

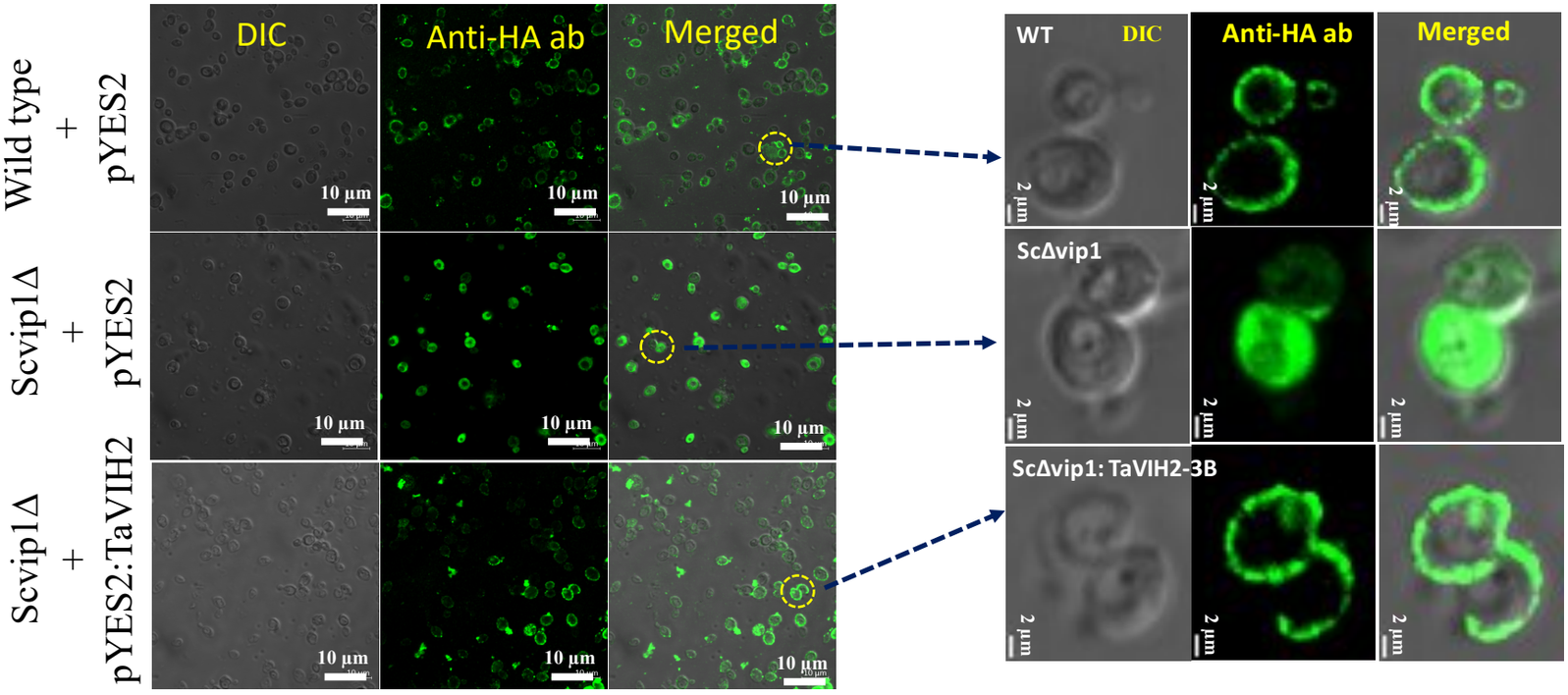
Wild type + pYES2
Scvip1Δ + pYES2
Scvip1Δ + pYES2:TaVIH2
DIC
Anti-HA ab
Merged
10 µm
WT
ScΔvip1
ScΔvip1: TaVIH2-3B
2 µm

Figure 4

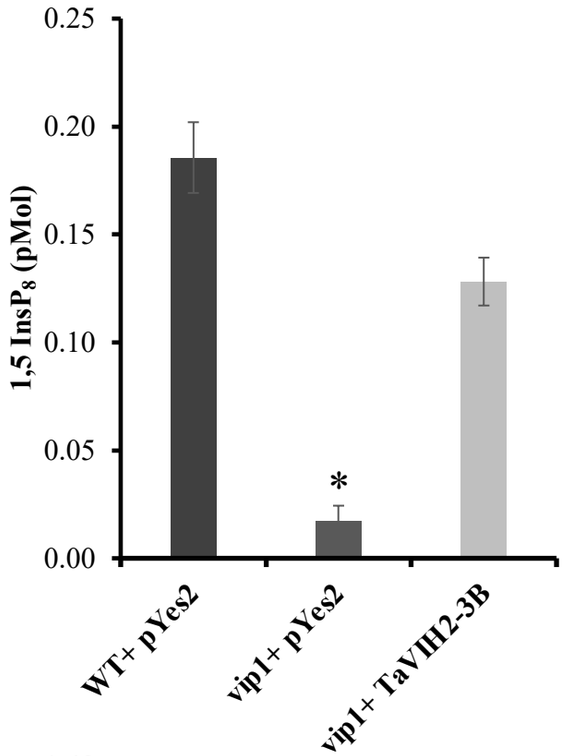
0.25
0.20
0.15
0.10
0.05
0.00
1,5 InsP8 (pMol)
*
WT+ pYes2
vip1+ pYes2
vip1+ TaVIH2-3B

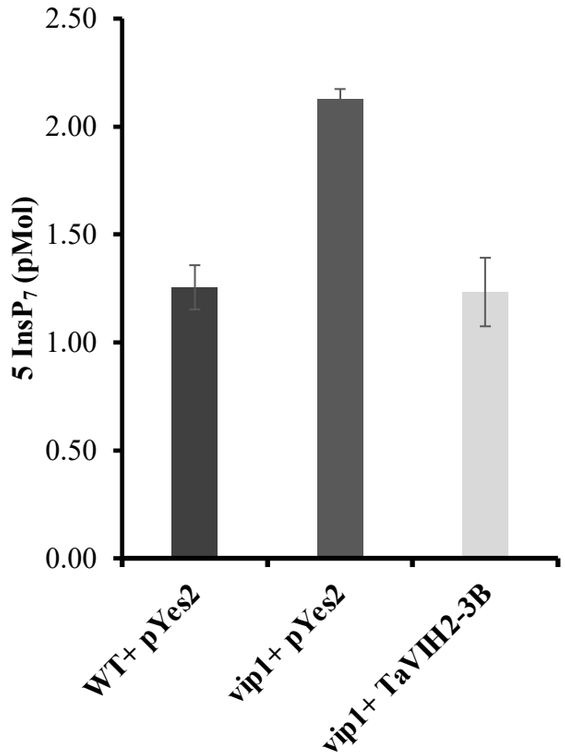
2.50
2.00
1.50
1.00
0.50
0.00
5 InsP7 (pMol)
WT+ pYes2
vip1+ pYes2
vip1+ TaVIH2-3B

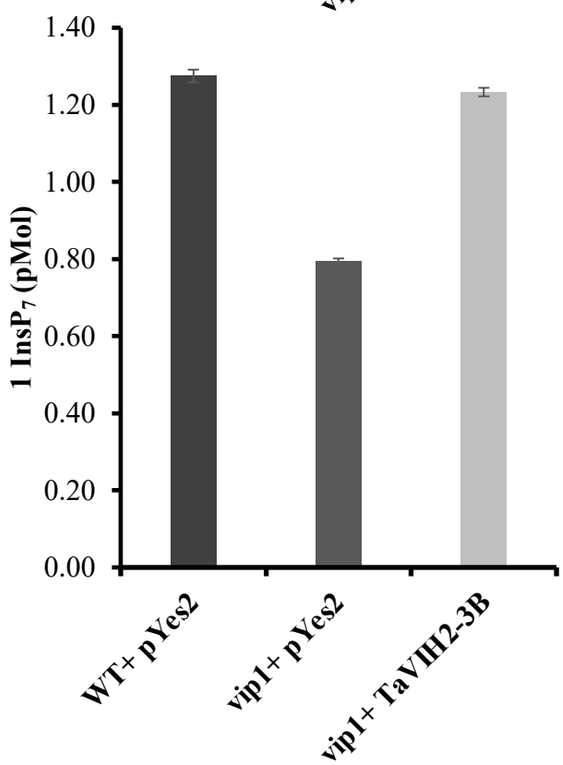
1.40
1.20
1.00
0.80
0.60
0.40
0.20
0.00
1 InsP7 (pMol)
WT+ pYes2
vip1+ pYes2
vip1+ TaVIH2-3B

Figure 5

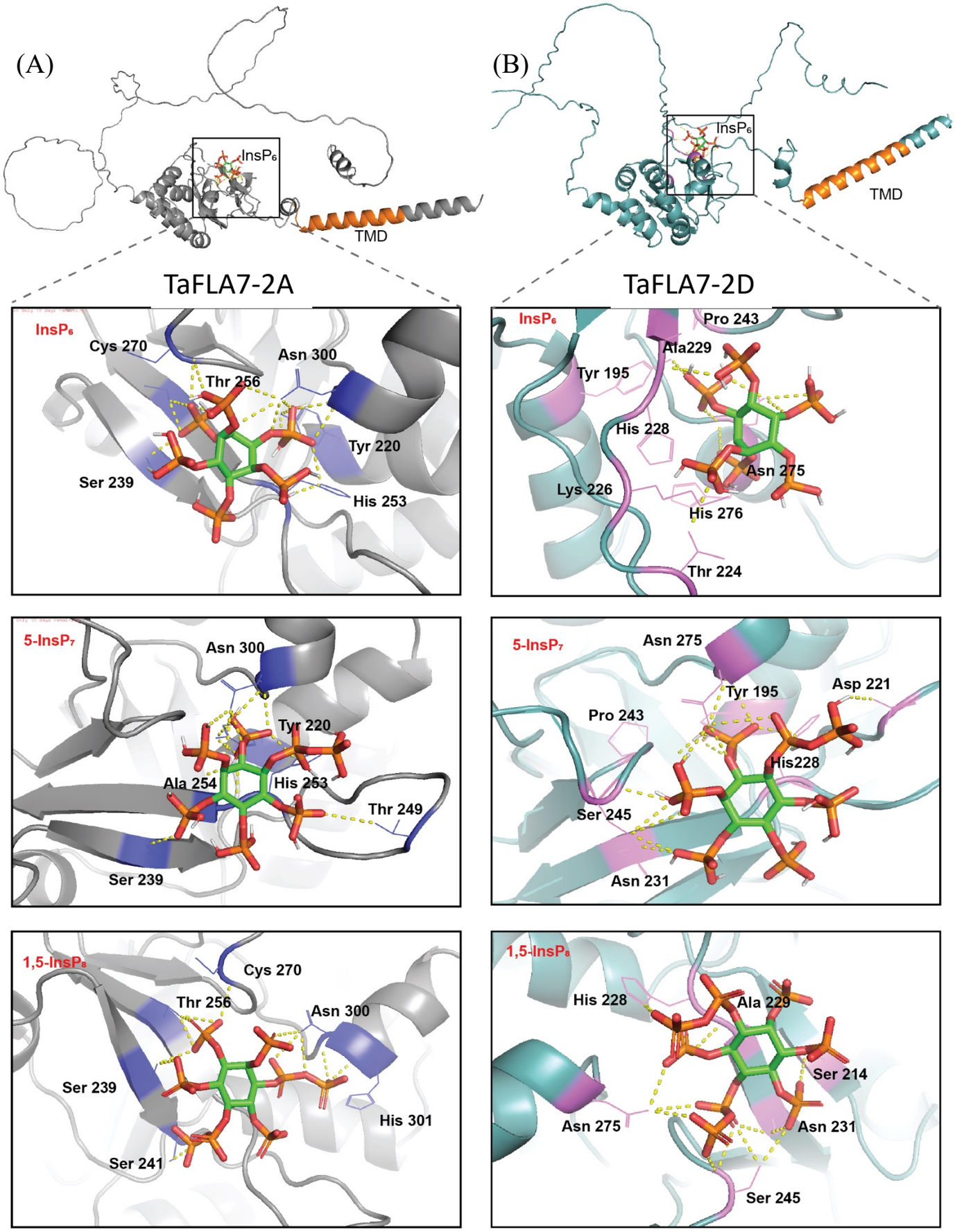
(A)
InsP₆
TMD
(B)
InsP₆
TMD
TaFLA7-2A
TaFLA7-2D
InsP₆
Cys 270
Asn 300
Thr 256
Tyr 220
Ser 239
His 253
InsP₆
Pro 243
Ala229
Tyr 195
His 228
Asn 275
Lys 226
His 276
Thr 224
5-InsP₇
Asn 300
Tyr 220
Ala 254
His 253
Thr 249
Ser 239
5-InsP₇
Asn 275
Tyr 195
Asp 221
Pro 243
His228
Ser 245
Asn 231
1,5-InsP₈
Cys 270
Thr 256
Asn 300
Ser 239
His 301
Ser 241
1,5-InsP₈
His 228
Ala 229
Ser 214
Asn 275
Asn 231
Ser 245

Figure 6

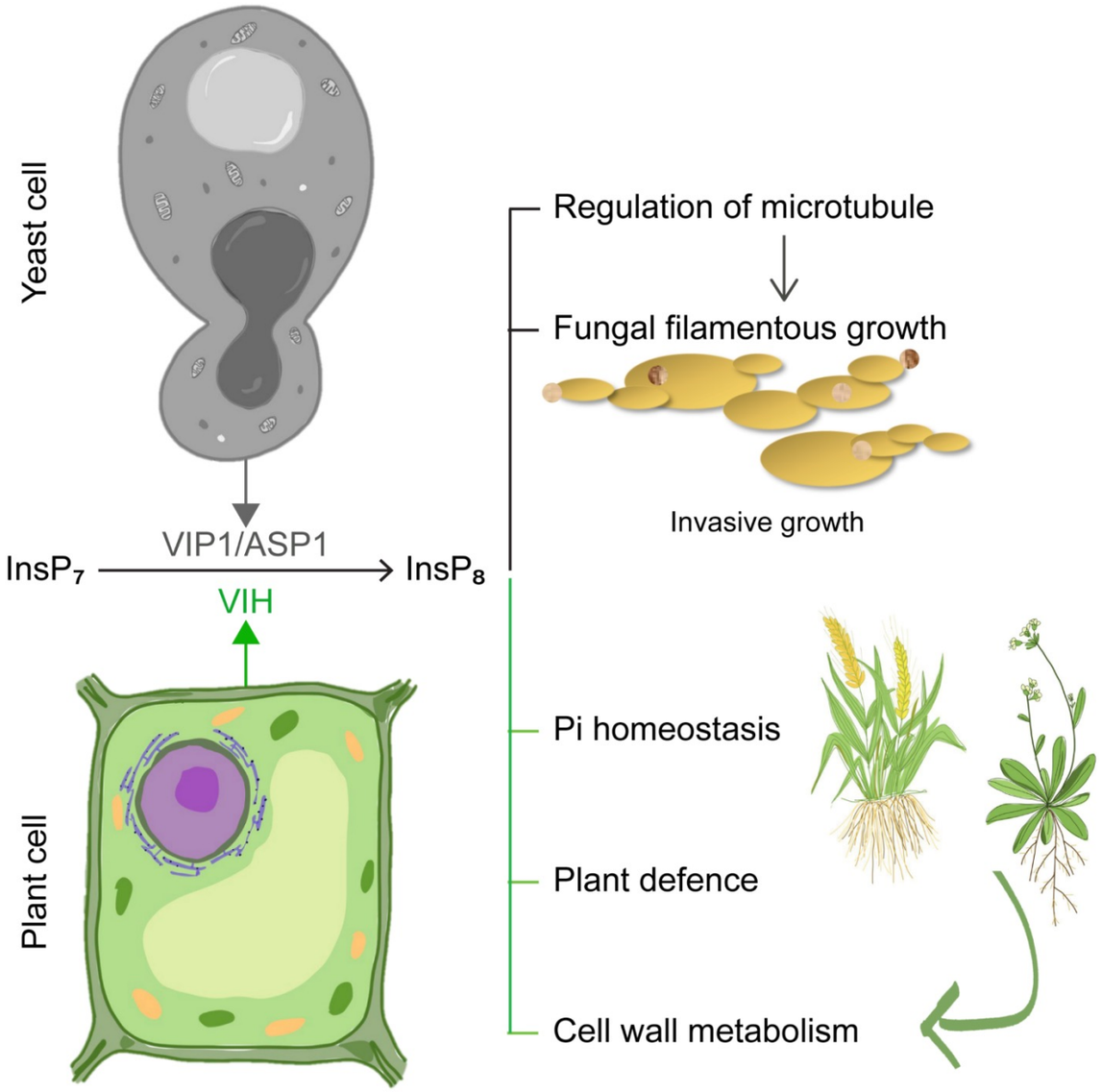
Yeast cell
VIP1/ASP1
InsP7
InsP8
VIH
Plant cell
Regulation of microtubule
Fungal filamentous growth
Invasive growth
Pi homeostasis
Plant defence
Cell wall metabolism

Figure 7